BJES Basrah Journal for Engineering Sciences

Basrah Journal for Engineering Sciences, Vol. 23, No. 2, 2023, 20-25

Original Article

Journal homepage: www.bjes.edu.iq
ISSN (Online): 23118385, ISSN (Print): 18146120

Prediction of Residual Stresses in 316 Stainless Steel Pipes Welded Joint

Zahraa A. Mutair[1,*] and Haider M. Mohammad[2]

[1] *Department of Mechanical Engineering, College of Engineering, University of Basrah, Basrah, Iraq*
[2] *Department of Material Engineering, College of Engineering, University of Basrah, Basrah, Iraq*
Email: eng.zahraa.alasadi@gmail.com, haider.mohammed@uobasrah.edu.iq

Received: 21 October 2022; Revised: 23 November 2022; Accepted: 1 December 2022; Published: 30 December 2023

Abstract:– Due to the extremely complicated thermal cycle for the welding process, the fusion zone and heat-affected zone (HAZ) produce irreversible elastic-plastic deformation and residual stresses. The differential heating of the pipes caused by the weld heat source causes residual stress as a result of the welding process. However, the strength and lifetime of the component are also decreased as a result of residual stresses in and around the weld zone. The objective of this research is to analyze the residual stresses created during the welding process and select the best welding parameters that give the lowest residual stresses in 316SS pipes with 50 mm diameter and 4 mm thickness that were manually welded by used (316) welding wire and using shielded metal arc welding (SMAW) in a single-pass butt joint with the various values for each of current (58, 68, 78, 88) amperes and voltage (22, 23, 24, 25, 26) volts. The shielded metal arc welding process involves heating, melting, and solidifying the parent metals and filler material in a localized fusion zone by a transient heat source to create a junction between the parent metals. The welding process free from preheating and heat treatment will be obtained. ANSYS Finite Element methods are used to calculate the welding residual stress distribution. The mechanical and thermal models were used to carry out the theoretical analysis. In general, the numerical study found that the residual stress distribution at the weld zone's center is continuous, rising, and has a value of about (1738 MPa). Additionally, the residual stress at the boundary between the heat-affected zone and the weld zone climbs to a maximum value of around (3799.6 MPa). On the other hand, the magnitude of the residual stress in the heat-affected zone of the weld reduces significantly and achieves a minimum value at a position of (20 mm) with a value near zero.

Keywords:– Stainless steel pipe weld, Residual stress, ANSYS, Finite element method, SMAW.

http://doi.org/10.33971/bjes.23.2.3

1. Introduction

Welding is a difficult process that is accompanied by shrinkage effects, phase transition, and the formation of residual stresses. Even when all external forces and temperature gradients beyond the yield point have also been reduced, residual stresses could still be found in a body [1]. Residue stresses, which may be relatively high, have a hazardous effect on the engineering parameters. During the welding process, heat from the process creates a localized expansion that is absorbed by the molten metal or the positioning of the components [2]. The stresses that remain within a component after an external load has been removed are known as residual stresses. Therefore, residual stress may be defined as any residual stress that persists in a process component that uses a mechanical or thermal approach without any imposed external loads. The expansion and contraction of the heat-affected zone and weld metal during local heating and subsequent cooling are the causes of residual stresses in welding. Without a doubt, residual welding stresses may cause stress-corrosion cracking and fatigue in particular conditions where such failure poses a risk [1, 3]. Some studies looked at how SMAW welding parameters, including weld current, weld time, electrode force, and surface condition of the components to be welded, affected the strength of SMAW welds made of the same materials. To measure the residual stresses, Prevéy [4] used the X-ray diffraction technique. While other earlier research focused on the effect of the welding process on residual stress [5], the effect of current and electrode type on metal's characteristics are studied by Moslemi et al. [6, 7]. Abdulkarim et al. (2019) built mathematical models for low-carbon steel plates based on experimental data to estimate the mechanical properties of submerged arc welding (SAW) [8]. A creative technique used in the theoretical study is to construct and solve two models, the first of which deals with the thermal analysis and the second with the mechanical analysis, and then link them together to simulate interactions between the two models using ANSYS software [9], this study is dedicated to choosing the best welding conditions that give the least residual stresses in 316 stainless steel welded pipes by the finite element method (FEM) using ANSYS software version 15.0 to simulate the transient thermal analysis and residual stresses analysis for SMAW welded specimens. The influence of both temperature dependence of material properties and heat generation value will be determined.

2. Simulation of residual stresses in welding 316 stainless steel pipe

The welding is a combined thermo-mechanical process. The residual stress field, however, is extremely dependent on the temperature field. The ANSYS finite element method is used to determine the distribution of welding residual stress. The process is composed of two steps: a thermal analysis as well as a mechanical analysis. The various analyses employed for the current investigation are described in the next subsections.

2.1. Analysis of thermal part

First, the governing partial differential equation for the three-dimensional transient heat conduction with internal heat production during welding is described by the thermal equilibrium equation [10].

$$\frac{\partial}{\partial x}\left(K_X\frac{\partial T}{\partial x}\right)+\frac{\partial}{\partial y}\left(K_Y\frac{\partial T}{\partial y}\right)+\frac{\partial}{\partial z}\left(K_Z\frac{\partial T}{\partial z}\right)+Q=\rho C\frac{\partial T}{\partial t} \tag{1}$$

Where: T is the temperature $^{\circ}C$, $^{\circ}K$ is the thermal conductivity (W/m.$^{\circ}C$), C is the specific heat (J/kg.$^{\circ}C$), ρ is the density (kg/m^3), t is the duration in (min), and Q is the rate of heat generation per unit volume (W/m^3). The thermal analysis uses the heat flux as the heat input over the weld bead [11].

$$Q_1=\frac{\eta\, I\, V}{A} \tag{2}$$

$$q=\frac{\eta\, I\, V}{S} \tag{3}$$

Where Q_1 represents the supplied heat flux (W/mm^2) from the welding arc on the workpiece's surface at any distance, q represents the arc power (J/mm), I represents the welding current (Amp), V represents the arc voltage (Volt), S represents the arc speed (mm/sec), A represents the weld bead area (mm^2), and η represents the thermal efficiency for SMAW welding.

The residual stress distribution of the weldment material is predicted by this simulation tool based on the value of metal volume changes that have been brought on by temperature fluctuation during the welding process. Heat input, the filler metal's travel speed, the weld pipe's thickness, the geometry, and the interpass's temperature are a few examples of such factors [12]. Accepting initial and boundary conditions results in the general solution to the differential equation explaining heat conduction in a solid body.

Initial conditions

$$t=0,\quad T_{w.m}=1350\ ^{\circ}C,\quad T_{workpiece}=30\ ^{\circ}C,\quad T_{air}=30\ ^{\circ}C$$

Boundary conditions

Surface convection and radiation will be the specific heat flow acting over the surface, according to:

$$K_n\frac{\partial T}{\partial n}=h(T_w-T_f)+\varepsilon\sigma(T_w^4-T_f^4) \tag{4}$$

Where h is the heat transfer coefficient at the workpiece's surface, T_w is the temperature of the workpiece's surface, T_f is the temperature of the surrounding, ε is the radiation coefficient of the black body, and σ is the Stefan–Boltzmann constant ($\sigma=5.67\times10^{-8}$ W/m^2.K).

Radiation and convection are both considered in order to take into account the heat losses from the surface of the welded pipe. Convection heat losses predominate away from the weld pool throughout the thermal cycle, while radiation heat losses are more prevalent within and around the weld pool. Eq. (5) utilizes the overall temperature-dependent heat transfer coefficient as opposed to estimating radiation and convection heat losses separately [13, 14].

$$h=\begin{cases}0.00668\ T & \left(\frac{W}{m^2,^{\circ}C}\right) \quad 0<T<500\\ 0.231\ T & \left(\frac{W}{m^2,^{\circ}C}\right) \quad T>500\end{cases} \tag{5}$$

2.2. Analysis of mechanical part

In the second stage of the study, the temperature histories that were computed by the prior thermal analysis for each time increment are used as an input (thermal loading) for a subsequent thermal stress analysis. The stress-strain ratio increases and the material transitions into a plastic condition as the melting temperature rises during the welding process. The isotropic Hooke's law, coupled with a temperature-dependent Young's modulus and Poisson's ratio, is used to compute the increases in elastic strain. Utilizing the coefficient of thermal expansion, the thermal strain increase is calculated. The elastic-plastic stress is calculated for the plastic strain increase using a rate-independent elastic-plastic constitutive equation with the Von Mises yield criteria, temperature-dependent mechanical properties, and the linear isotropic hardening rule:

$$[d\sigma]=[D^{ep}]d\varepsilon_{ij}-[C^{th}]dT \tag{6}$$

$$d\varepsilon_{ij}=d\varepsilon_{ij}^{e}+d\varepsilon_{ij}^{p}+d\varepsilon_{ij}^{th} \tag{7}$$

$$[D^{ep}]=[D^{e}]+[D^{p}] \tag{8}$$

Where, $d\varepsilon_{ij}^{e}$ is the elastic strain increment, $d\varepsilon_{ij}^{p}$ is the plastic strain increment, $d\varepsilon_{ij}^{th}$ is the thermal strain increment, $[D^e]$ is the elastic stiffness matrix, $[D^p]$ is plastic stiffness matrix, $[C^{th}]$ is thermal stiffness matrix, dT is the temperature increment, and $[D^{ep}]$ is elastic-plastic stiffness matrix [15].

2.3. Material properties

welding procedures take place at very high-temperature cycles and show temperature-dependent properties of materials. It is a widespread assertion in the literature that if future advancements in numerical modeling of welding processes are to be made, extra emphasis must be devoted

to the description of the material properties and its behavior. But it is also clear that the model and pertinent properties just need to be accurate enough to reflect the true material behavior [16].

Due to the lack of information on the material properties of weld metal and heat-affected zone, the material studied in this research is stainless steel pipe. As a result, both the thermal and mechanical material properties of the weld metal and heat-affected zone are assumed to be the same as those of the base metal. Tables provide an explanation of the material properties change with the temperature (1, 2, 3, 4, 5, 6, 7).

Table 1: density of 316SS as a function of temperature [16].

No.	Temperature (°C)	Density (Kg/m³)
1	20	7950
2	90	7920
3	200	7880
4	320	7830
5	430	7790
6	540	7740
7	650	7690
8	760	7640
9	870	7590

Table 2: thermal expansion of 316SS as a function of temperature [16].

No.	Thermal expansion	Temperature (°C)
1	15.156	27
2	16.051	127
3	16.933	227
4	17.511	327
5	17.946	427
6	18.297	527
7	18.592	627
8	18.847	727

Table 3: thermal conductivity of 316SS as a function of temperature [16].

No.	thermal conductivity (W/m°C)	Temperature (°C)
1	13.5	200
2	16	400
3	18.5	600

Table 4: modulus of elasticity of 316SS as a function of temperature [16].

No.	Modulus of elasticity (GPa)	Temperature (°C)
1	194.04	90
2	185.22	200
3	176.4	230
4	163.66	430
5	156.8	540
6	147.98	550
7	137.2	760

Table 5: specific heat of 316SS as a function of temperature [16].

No.	Specific heat (J/Kg.°C)	Temperature (°C)
1	452	20
2	486	90
3	528	200
4	548	320
5	565	430
6	573	540
7	586	650
8	615	760
9	649	870

Table 6: Poisson's ratio of 316SS as a function of temperature [16].

No.	Poisson's ratio	Temperature (°C)
1	0.26	150
2	0.29	260
3	0.34	370
4	0.3	480
5	0.32	590
6	0.31	700
7	0.24	820

Table 7: Resistivity of 316SS as a function of temperature [16].

No.	Resistivity (Ω m)	Temperature (°C)
1	7.40E-07	20
2	7.90E-07	90
3	8.70E-07	200
4	9.30E-07	320
5	9.90E-07	430
6	1.04E-06	540
7	1.10E-06	650

2.4. Numerical analysis

The Finite Element approach is used in the ANSYS software to simulate the SMAW welding process. Figure 1 schematically illustrates the geometry and dimensions of a pipe butt weld manufactured of stainless steel pipe with an outer diameter of 50 mm, a thickness of 4 mm, and a length of 200 mm [17]. Figure 2 shows the design of the face sample that be welded with 37° angle ($AWS-D10.4-86$) [18] to reduce the volume of weld metal. For better control of weld quality in the root bead through the use of SMAW. The Finite Element welding procedure is carried out in two

stages: transient heat analysis and static structural analysis. In the simulation model, the mesh size was chosen based on an analysis of the elements' sensitivity, where several values were taken for mesh size and the value that gives stable temperature values. Therefore, it was investigated how many pipes may be displaced at once during welding. The maximum number of nodes is equal to 97723 when the number of elements is equal to 17376, as shown in Fig. 3. Single-pass welding is used to join the pipe using the following welding parameters, SMAW welding procedure, welding currents of 58, 68, 78, and 88 amps, and welding voltages of 22, 23, 24, 25, and 26 volts [17] The austenitic stainless steel pipe (316SS) was the material employed in this project.

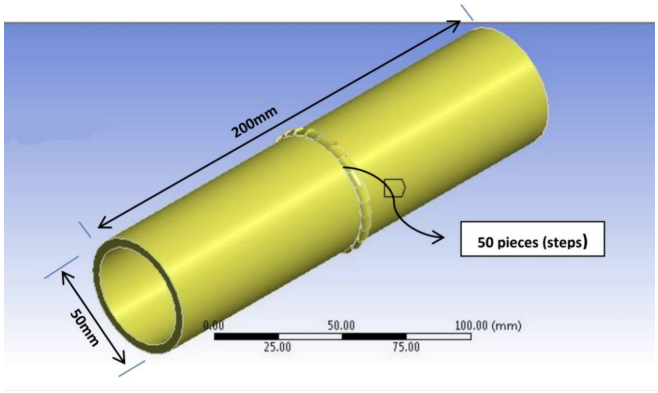

Fig. 1: dimensions of analysis sample.

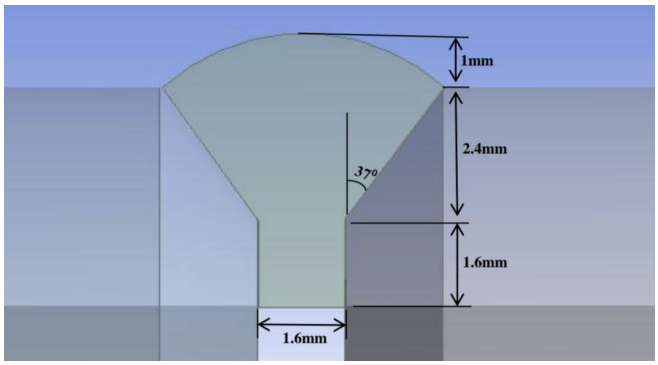

Fig. 2: Joint design of analysis sample (AWS-D10.4-86) [17].

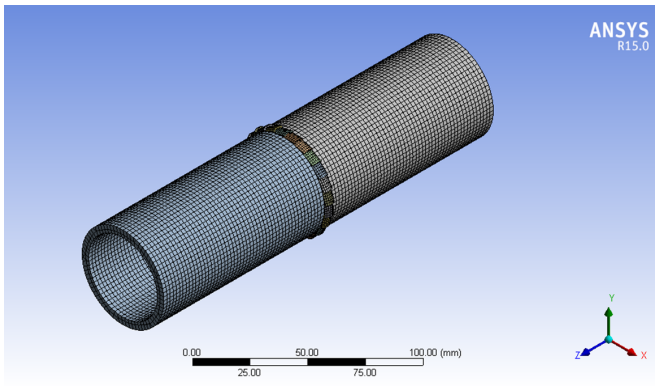

Fig. 3: Mesh size used in analysis of the FEM.

3. Results and discussion

The main objective of this work was to create a dependable FEM model that could more accurately anticipate the thermal history and residual stresses of a stainless steel pipe weld. The residual stress measured by ANSYS is (3799.6 MPa) at the welding center (zero mm), and the results of the FEM created from the welding centerline to the pipe edge are shown in Figs. 4 and 5. Due to the material's resistance to contraction when cooling begins, areas surrounding the weld experience more residual stress than the welding center, which subsequently increases before falling to a lower magnitude. In general, the numerical study found that the residual stress distribution at the weld zone's center is continuous, rising, and has a value of about (1738 MPa). Additionally, the residual stress at the boundary between the heat-affected zone and the weld zone climbs to a maximum value of around (3799.6 MPa). On the other hand, the magnitude of the residual stress in the heat-affected zone of the weld reduces significantly and achieves a minimum value at the position of (20 mm) with a value near zero. This description of the residual stress on the stainless steel pipe sample is seen with great resemblance to the side centerline welding.

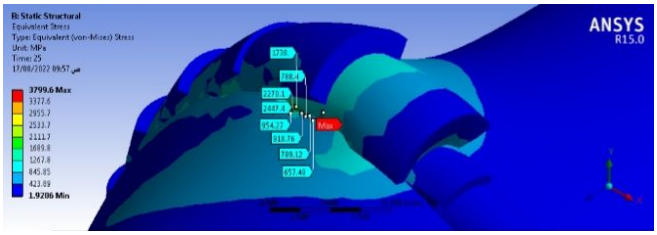

Fig. 4: Residual Stresses at current 58 A, voltage 22 V.

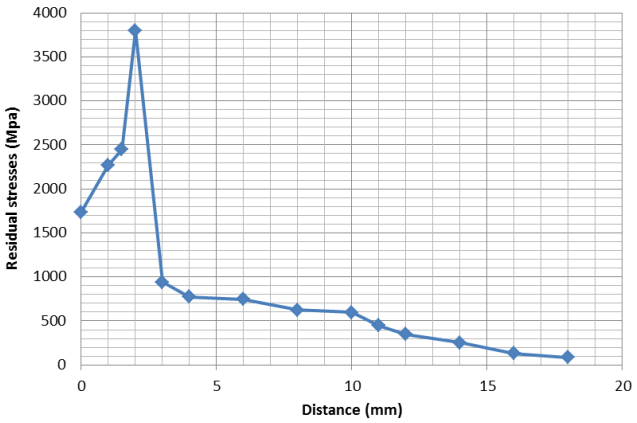

Fig. 5: Residual stresses from the welding centerline.

4. FEM model validation for residual stresses

The main objective of this work was to create an accurate FEM modal that could forecast the thermal history and residual stresses of a stainless steel pipe weld with greater accuracy. The behavior of the experimental findings of the researcher Miftin et al. [9] and the behavior of the results

of the numerical model are known to be in fairly good agreement, simple discrepancies can result. Figure 6 shows the experimental and theoretical results from the welding centerline to the pipe edge obtained by the researcher above. High residual stress is seen at the welding center, increasing in areas surrounding the weld owing to a resistive shrinkage of the material when cooling begins, and then reducing until it achieves a lower magnitude.

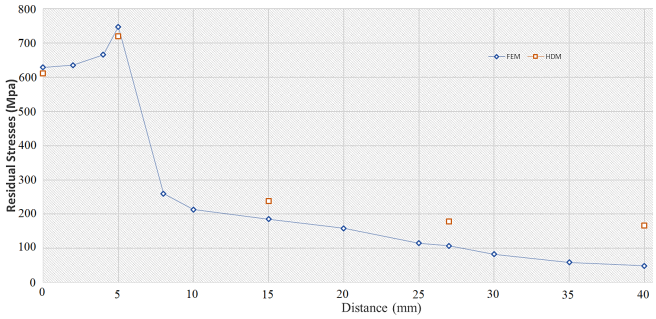

Fig. 6: The experimental and theoretical results from welding centerline to the pipe edge [9]

4.1. Change in voltage affects residual stress

Figure 7 illustrates the residual stress fields for welding voltages of 22, 23, 24, 25, and 26 volts that were employed in the simulations. When the welding voltage increases, the heat input energy increases, which is a function of welding voltage. The degree of generated residual tensions has thereby grown, it might be said.

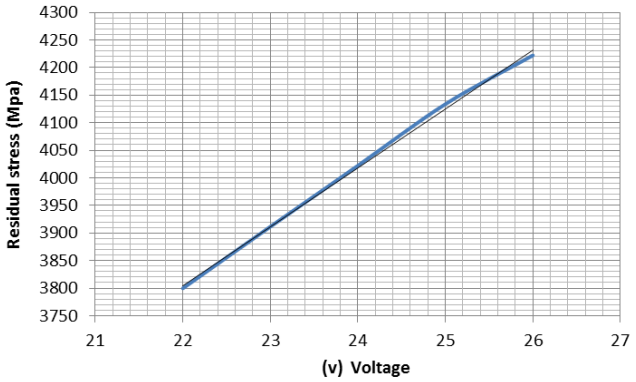

Fig. 7: the effect of the voltage change on the residual stresses.

4.2. Changes in amperage affect residual stress

Figure 8, which holds all other variables constant, displays the residual stress on the pipe's outer surface for four different currents of 58, 68, 78, and 88 Amp. The total amount of input heat rises as the amperage increases. When the linear welding speed and all other variables are maintained constant, the impacts of input heat directly affect the temperature distribution and the ensuing residual stress graph in welded structures.

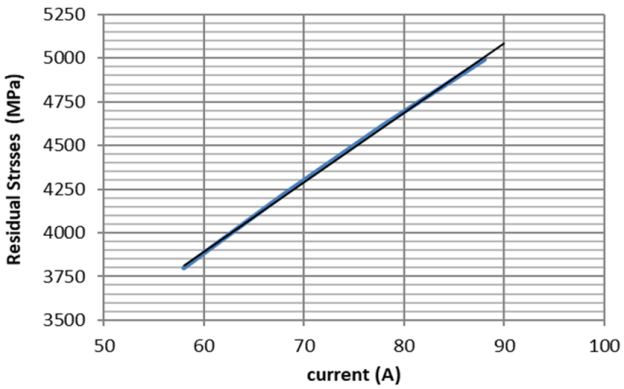

Fig. 8: the effect of the amperage change on the residual stresses.

As a consequence of the ANSYS program's findings, the equations that depict the residual stresses eq. (9) and temperature distribution eq. (10) for any amount of current and voltage in the weld metal be formed, and it may be written as follows:

$$R.S. = 34.901\,(I \times V)^{0.655786} \tag{9}$$

$$T = 2.7426\,(I \times V)^{0.88} \tag{10}$$

5. Conclusions

the amount of residual stresses in stainless steel pipe welding was estimated using a FEM model. The effect of mechanical properties, alloy material, and environmental factors were included in the amount of residual stresses. From the previous analysis, it can be shown that the calculated properties of residual stresses for a specific system depend on the values of the parameters, and the most important conclusions that can be drawn from the present study are as follows:

1. Reducing the residual stress in welding by using the lowest current and voltage, thus reducing the amount of heat input in the weld.
2. The surface between the fusion zone and heat-affected zone is susceptible to failure that results from welding residual stress.
3. The maximum residual stress occurred in the region near the fusion zone, increasing with a decreasing specimen thickness.
4. The increase in temperature that results from heat input leads to the residual stress values increase.

Nomenclature		
Symbol	**Description**	**SI Units**
T	Temperature	°C
K	Thermal conductivity	W/m.°C
c	Specific heat	J/kg.°C
t	Time duration	min
Q	Rate of heat generation per unit volume	W/m³
q	Arc power	J/mm
I	Welding current	Amp
V	Arc voltage	Volt
S	Arc speed	mm/sec
A	Weld bead area	mm²
h	Heat transfer coefficient at the workpiece's surface	W/m².°C
T_w	Temperature of the workpiece's surface	°C
T_f	Temperature of the surrounding	°C
D^e	Elastic stiffness matrix	-
D^p	Plastic stiffness matrix	-
D^{ep}	Elastic-plastic stiffness matrix	-
C^{th}	Thermal stiffness matrix	-
dT	Temperature increment	-
Greek Symbols		
Symbol	**Description**	**SI Units**
ρ	The density	kg/m^3
η	Thermal efficiency for SMAW welding	-
ε	Radiation coefficient of the black body	-
σ	Stefan–Boltzmann constant ($\sigma = 5.67 \times 10^{-8}$ W/m^2.K)	W/m².K
$d\varepsilon_{ij}^e$	Elastic strain increment	-
$d\varepsilon_{ij}^p$	Plastic strain increment	-
$d\varepsilon_{ij}^{th}$	Thermal strain increment	-

References

[1] T. Gurova, C. U. E. da Zona Oeste, X. Castello, H. do Brasil, and S. F. Estefen, "Analysis of residual stress state in welded steel plates by x-ray diffraction method," *Rev. Adv. Mater. Sci*, vol. 19, pp. 172–175, 2009.

[2] A. N. Al-Khazraji, S. A. Al-Rabii, and A. H. F. Al-Jelehawy, "Fe analysis of residual stresses induced by spot welding of stainless steel type aisi 316," *Engineering and Technology Journal*, vol. 32, no. 2 Part (A) Engineering, 2014.

[3] A. A106, "Standard specification for seamless carbon steel pipe for high-temperature service," 2006.

[4] P. S. Prevéy, "X-ray diffraction characterization of residual stresses produced by shot peening," *Shot Peener(USA)*, vol. 15, no. 1, pp. 4–8, 2001.

[5] H. Alipooramirabad, A. Paradowska, R. Ghomashchi, and M. Reid, "Investigating the effects of welding process on residual stresses, microstructure and mechanical properties in hsla steel welds," *Journal of Manufacturing Processes*, vol. 28, pp. 70–81, 2017.

[6] N. Moslemi, N. Redzuan, N. Ahmad, and T. N. Hor, "Effect of current on characteristic for 316 stainless steel welded joint including microstructure and mechanical properties," *Procedia CIRP*, vol. 26, pp. 560–564, 2015.

[7] M. Mosaad and S. S Mohamed, "Effect of electrode type on the characteristics of aisi 316 stainless steel," *Engineering Research Journal-Faculty of Engineering (Shoubra)*, vol. 44, no. 1, pp. 5–9, 2020.

[8] A. K. F. Hassan, R. J. Jasim, and Y. Y. Ashoor, "Estimation of submerged arc plates weldment properties using anfis and regression techniques," *Basrah Journal for Engineering Sciences*, vol. 20, no. 2, 2020.

[9] S. S. Miftin, H. M. Mohammed, and A. A. Nassar, "Measurement and prediction of residual stresses in low carbon steel pipes welded shielded metal arc welding," *Basrah J. Eng. Sci*, vol. 20, no. 2, pp. 60–65, 2020.

[10] J. Dhas and S. Kumanan, "Weld residual stress prediction using artificial neural network and fuzzy logic modeling," 2011.

[11] ASTM, "Standard for welding and brazing procedures, welders, braziers, and welding and brazing operators," 2004.

[12] T.-L. Teng and C.-C. Lin, "Effect of welding conditions on residual stresses due to butt welds," *International Journal of Pressure vessels and piping*, vol. 75, no. 12, pp. 857–864, 1998.

[13] K.-H. Chang, C.-H. Lee, K.-T. Park, Y.-J. You, B.-C. Joo, and G.-C. Jang, "Analysis of residual stress in stainless steel pipe weld subject to mechanical axial tension loading," *International Journal of Steel Structures*, vol. 10, pp. 411–418, 2010.

[14] B. Brickstad and B. Josefson, "A parametric study of residual stresses in multi-pass butt-welded stainless steel pipes," *International Journal of pressure Vessels and piping*, vol. 75, no. 1, pp. 11–25, 1998.

[15] R. Dieter, "Heat effects of welding temperature field, residual stress, distortion," 1992.

[16] B. S. S. Association *et al.*, "Elevated temperature physical properties of stainless steels," 2016.

[17] M. E. Abdulhadi, "Effect of arc welding parameters on the mechanical properties and microstructure of 316 stainless steel pipes using experimental work and neural networks," Master's thesis, Mechanical Engineering Dep., College of Engineering; University of Basrah, Basrah, Iraq, 2014.

[18] A. W. S. C. on Piping and Tubing, *Recommended Practices for Welding Austenitic Chromium-nickel Stainless Steel Piping and Tubing*. American Welding Society, 1986.